

SciEn Conference Series: Engineering Vol. 3, 2025, pp 331-336

https://doi.org/10.38032/scse.2025.3.94

Influence of Dimple Orientation on Drag Characteristics of Circular Cylinder at Subsonic Flow

Md. Shahjahan Durjoy^{I,*}, Sneha Sadia Tarannum²

Department of Mechanical and Production Engineering, Ahsanullah University of Science and Technology, Dhaka, Bangladesh Department of Smart Health Science & Technology, Kangwon National University, Chuncheon, South Korea

ABSTRACT

This study investigates the drag reduction potential of a cylinder with combinations of dimpled and smooth surfaces, examining the effects of various dimple placements on drag coefficient (C_D) across a range of Reynolds Numbers (Re). Experimental results reveal that strategic dimple placements on the cylinder's windward side effectively reduce drag by influencing boundary layer behavior. Specifically, the configurations with 60° dimpled and 150° smooth and 120° dimpled and 60° smooth surfaces consistently demonstrated the lowest drag coefficients, especially at higher Reynolds Numbers, where delayed flow separation was achieved. Conversely, configurations with limited dimple coverage, such as 30° dimpled and 150° smooth, produced higher drag coefficients, indicating less effective boundary layer control. Full dimple coverage (180° dimpled) showed significant drag reduction only at higher Reynolds Numbers, while higher drag persisted at lower speeds. These findings suggest that partial dimple coverage on the windward side can optimize drag reduction by promoting early boundary layer transition, making such configurations advantageous for applications requiring efficient aerodynamic and hydrodynamic performance. The overall results indicate that dimple placement is crucial in influencing drag, providing insights for optimizing surface modifications for improved aerodynamic efficiency.

Keywords: Bluff-body drag reduction, Circular cylinder, Dimple orientation, Passive drag reduction, Drag characteristics.



Copyright @ All authors

This work is licensed under a Creative Commons Attribution 4.0 International License.

1. Introduction

From 1851 to 2021, the cumulative global emissions of 2,471 billion metric tons CO₂, lead to a CO₂-induced increase in global mean surface temperature of 1.11°C. Out of this, only fossil emissions contributed 1,732 billion metric tons of CO₂ emission, causing a warming of 0.78°C increase [1]. Fossil fuels still remain the predominant method of energy extraction globally despite the introduction of renewable sources. Reducing energy consumption is the key strategy for minimizing energy production through the burning of fossil fuels. One effective way to achieve this is by decreasing the drag experienced by various objects, which can significantly lower energy demands. Bluff bodies are seen in various engineering applications, such as automobiles [2], marine vessels [3], high-rise buildings and bridge piers [4,5], high-speed trains [6], aircraft [7] etc. These exemplify both dynamic and stationary bluff bodies, where drag force is a critical design factor. From the perspective of fluid dynamics, drag force on the bluff bodies plays a key factor in determining the consumption of energy throughout different applications. In simpler terms, the resistance of these bodies in fluid flow is directly related with the energy cost. A larger drag coefficient requires extra energy consumption leading to more fuel cost, industrial process cost, and operational cost, and also results in heightened emissions. Thus, the reduction in energy consumption contributes to the preservation of the environment by curbing fossil fuel dependency and reducing harmful emissions.

In the last few decades, researchers have employed both active and passive techniques to mitigate bluff body drag by

altering the boundary layer or the resulting wake. The circular cylinder has long been considered a classic bluff body for experimentation, with numerous studies conducted to predict the variation of drag as a function of Reynolds number.

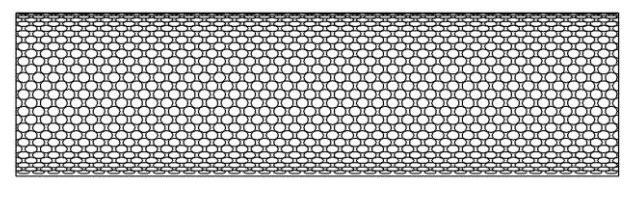
In the thorough investigation conducted by Bearman et al. [8], they attributed the drag reduction effect of dimples to the trailing vortices generated by each dimple, which energize the boundary layer and delay flow separation, resulting in enhanced drag reduction. Howard et al. [9] observed that circumferential grooves could achieve up to a 50% drag reduction with a laminar boundary layer, demonstrating the influence of surface textures on drag outcomes. In the work of Tay [10], they observed that drag reduction due to dimples only becomes significant at Reynolds numbers above 25,000, achieving a peak reduction of about 0.7% at 30,000. Eng et al. [11] investigated the drag reduction properties of circular dimples in turbulent flow and found that shifting the deepest point downstream by 0.1 diameter from the center provided the greatest reduction in drag, highlighting the potential of precise geometric adjustments in passive drag reduction applications. Lienhart et al. [12] examined the effect of shallow dimples arranged on a channel wall and observed up to a 20% reduction in skin-friction drag, indicating the potential for dimples to reduce drag in turbulent flows. Klausmann et al. [13] conducted experiments on circular cylinders coated with a porous layer on the leeward side, observing that the porous layer

increased base pressure, leading to reduced drag and dampened oscillation amplitudes, which supports the effectiveness of passive coatings in drag management for circular geometries. Van Nesselrooij et al. [14] tested flat surfaces with shallow dimples and observed a drag reduction of up to 4%, which was maximized at a Reynolds number of 40,000, demonstrating the potential of dimpled surfaces to reduce drag in turbulent flows. Choi et al. [15] examined a dimpled sphere and observed that dimples initiate shear layer instability and turbulence within the boundary layer, contributing to flow reattachment and delaying separation, which effectively reduces drag. Then, Butt et al. examined circular cylinders with outwardly pressed hexagonal patterns, finding that these patterns reduced the drag coefficient to 65% of that for a smooth cylinder, highlighting the effectiveness of hexagonal pattern orientation for drag reduction. Through PIV analysis, Zhou et al. [16] documented that the dimpled surface on a circular cylinder weakened vortex shedding, reducing oscillation strength and contributing to drag reduction. They found that the dimpled circular cylinder exhibited lower turbulent kinetic energy in the wake compared to the smooth cylinder, pointing to reduced shear layer interactions as a mechanism for drag reduction. Yan et al. [17] analyzed a circular cylinder with a fully dimpled surface and observed that within a certain Reynolds number range, the dimpled structure achieved a maximum drag reduction rate of 19%, illustrating the potential for significant drag reduction in turbulent flow conditions. While previous studies have explored the effects of dimples on drag reduction, few have systematically examined the influence of varying dimple placements on the drag coefficient (C_D) across a range of Reynolds numbers. The current work primarily focuses on the effect of dimples, conducting detailed investigations into optimal dimple and smooth surface configurations, and exploring the interaction between dimpled and smooth surface areas.

For the experimentation, a circular cylinder was designed, which has dimples on the 180° of its outer surface, and the other half was kept smooth. In the present study, it was investigated how different dimple orientations, meaning different combinations of dimpled surface and smooth surface influence the drag characteristics of circular cylinders at subsonic Flow. Tay [10] found that depending on the Reynolds number, a depth-to-diameter ratio of 5 percent located in a channel was experimentally found to affect drag. Van Nesselrooij et al. [14] have tested several dimple depths and found that for the purposes of drag reductions, the depth-to-diameter ratio (d/D) should be below 10 percent. However, from the manufacturing point of view, it was not possible to print those precise dimples, so the depth-to-diameter ratio for this experiment was about 18 percent. Here, the diameter of the cylinder was selected as 24 mm. Dimples were introduced on the surface of the cylinder with a depth (d) of 0.276 mm and a diameter (D) of 1.526 mm, aiming to modify the surface flow characteristics and potentially reduce aerodynamic drag.

The design of the dimple array was inspired by Tay [10]; whose research focused on wall surfaces where the design demonstrated drag-reducing effects at different Reynolds

numbers. **Figure 1** shows the drawing for the cylinder with dimples. The dimples are placed in half of the cylinder, i.e., 180° . **Figure 2** shows the dimple configuration, which covers half of the cylinder again. Finally, the fabricated 3D printed cylinder is shown in **Figure 3**.



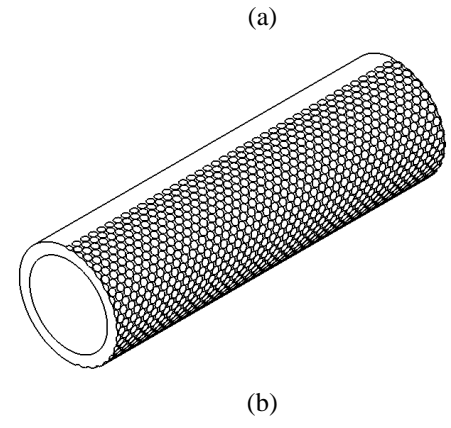


Fig.1 The dimpled surface of the circular cylinder, (a) Frontal view of the dimpled surface, (b) Isometric view of the cylinder

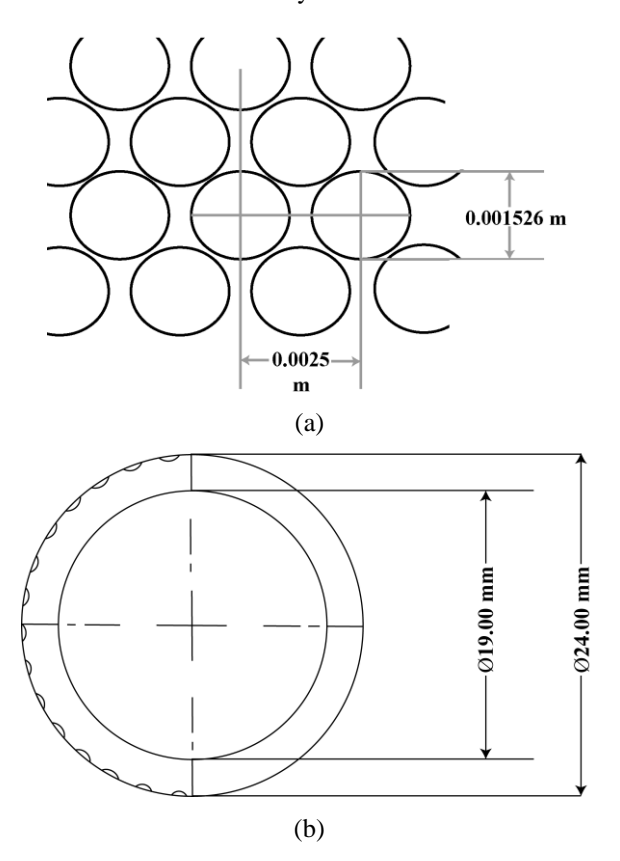


Fig.2 (a) Space between two dimples, (b) Inner and outer diameter of the cylinder



Fig.3 3D printed cylinder

2. Experimental Setup

Experimental investigations were conducted using the TecQuipment AF100 subsonic wind tunnel. The wind tunnel operates within a velocity range of 0 to 36 m/s, with an RMS value below 0.03%, a standard deviation of the mean velocity under 1%, and a maximum fluctuation of 4% in the freestream velocity. Also, the blockage ratio of the test section is kept below 10 percent. The dimension of the test section of the wind tunnel is $30.5 \text{ cm} \times 30.5 \text{ cm} \times 60 \text{ cm}$. The velocity (V_{∞}) is measured using the formula below, based on readings from the manometer-connected pitot-static tube located upstream of the wind tunnel's test section,

$$V_{\infty} = \sqrt{\frac{2 \,\rho_{mf} \,g \,H_{air}}{\rho_{air}}} \tag{1}$$

Where, V_{∞} is the velocity of air in the wind tunnel, ρ_{mf} and ρ_{air} is the density of manometric fluid (CCL₄) and air respectively, g is the acceleration due to gravity and H_{air} is the manometric column height of air. The overall drag force for each arrangement was directly measured using an AF1300Z Balance Assembly. Then, the drag coefficient was calculated using,

$$C_D = \frac{F_D}{\frac{1}{2} \rho_{air} A V_{\infty}^2} \tag{2}$$

The setup is illustrated in **Fig.4**. The cylinder was held onto the supporting rod horizontally connected to the fixed end of the wind tunnel and was kept perpendicular to the incoming airflow in the test section. For at least 30 seconds, all force measurements were acquired. The separate control unit is used to regulate the axial fan speed, thereby controlling the velocity of air in the wind tunnel's test area. The cylinder was set for six different velocities in seven different positions.

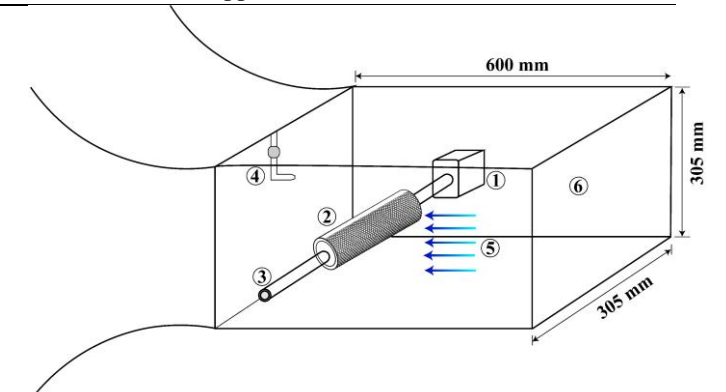


Fig.4 Wind Tunnel Setup: (1) Strain-gauge load cell (for drag and lift measurement), (2) Cylinder, (3) Dummy arm (for flow symmetry), (4) Pitot-static tube, (5) Direction of flow, (6) Wind tunnel test-section

The different combinations of the dimpled surface and smooth surface were tested as follows:

- 1) 0° of the dimpled surface on the windward side and 180° smooth surface on the leeward side
- 2) 30° of the dimpled surface on the windward side and 150° of the smooth surface on the leeward side
- 3) 60° of the dimpled surface on the windward side and 120° of the smooth surface on the leeward side
- 4) 90° of the dimpled surface on the windward side and 90° of the smooth surface on the leeward side
- 5) 120° of the dimpled surface on the windward side and 60° of the smooth surface on the leeward side
- 6) 150° of the dimpled surface on the windward side and 30° of the smooth surface on the leeward side
- 7) 180° of the dimpled surface on the windward side and 0° of the smooth surface on the leeward side

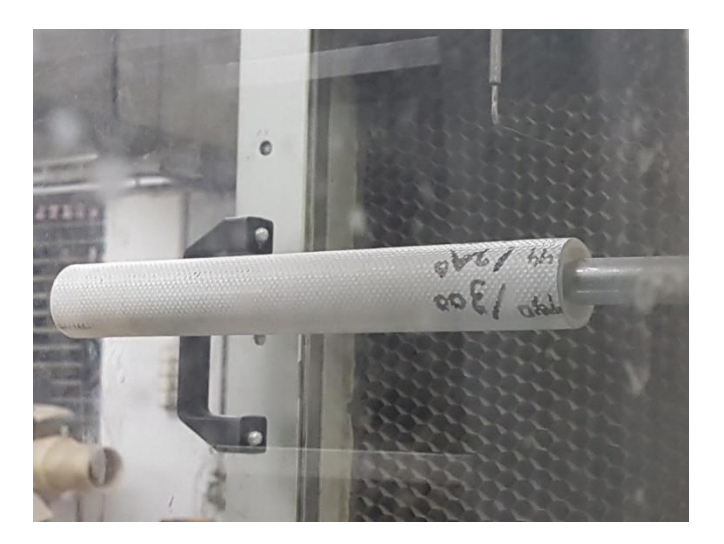
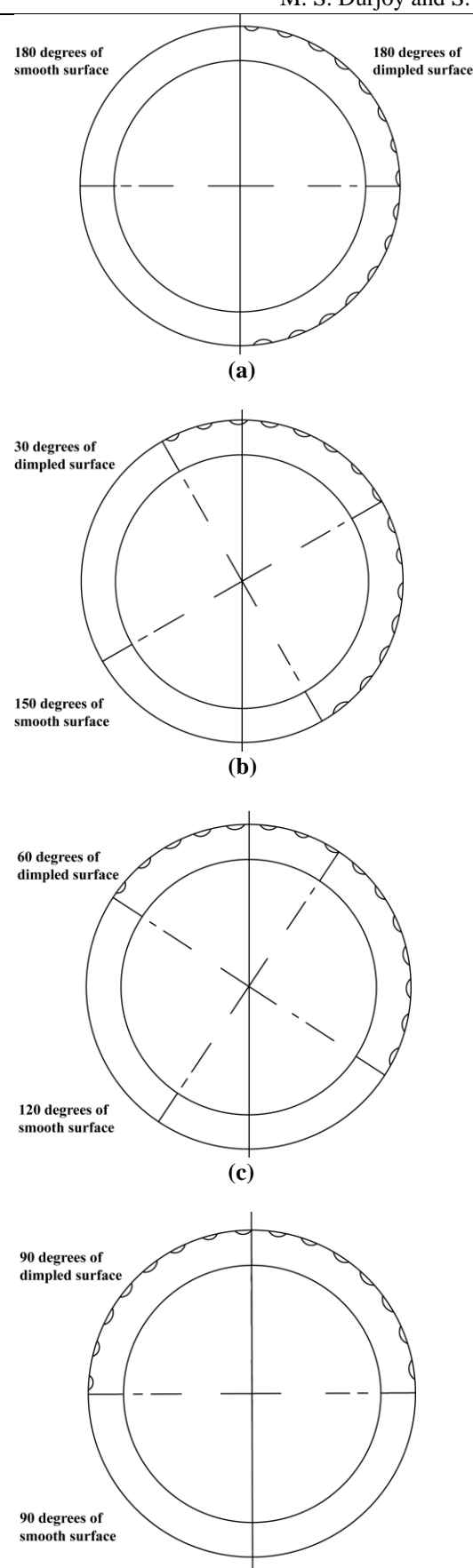


Fig.5 Setup of the cylinder on the test stem in the test section of the wind tunnel

The cross-sections of different combinations of the dimpled surface and smooth surface which are tested are depicted in ${\bf Fig.~6}$



(d)

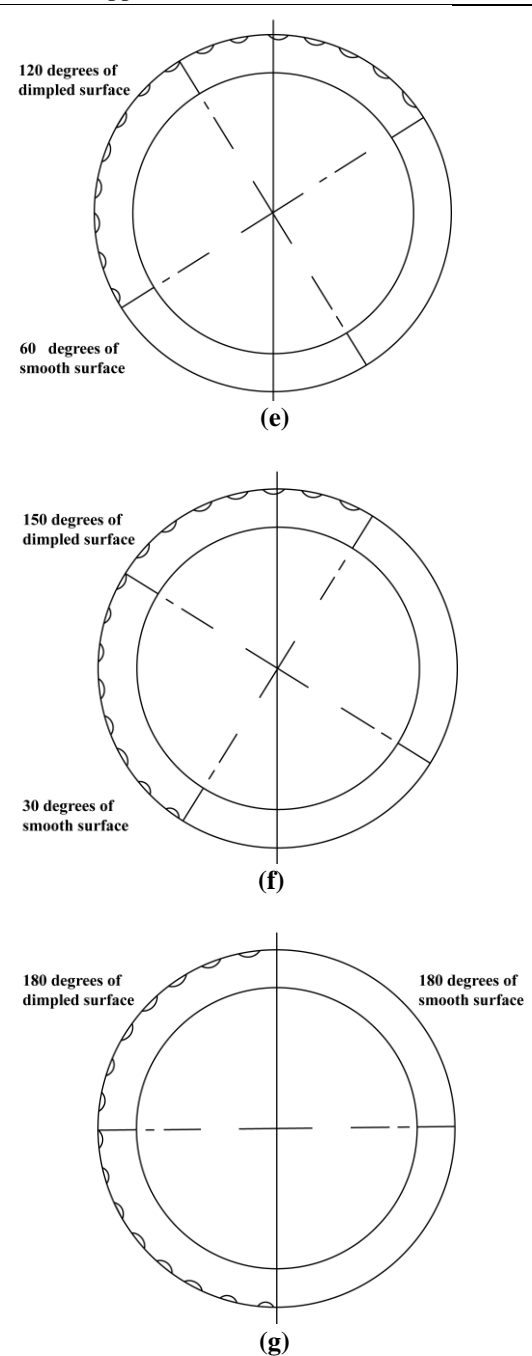


Fig.6 (a) 1st Position (0° dim. 180° sm.), **(b)** 2nd position (30° dim. 150° sm.), **(c)** 3rd position (60° dim. 120° sm.), **(d)** 4th position (90° dim. 90° sm.), **(e)** 5th position (120° dim. 60° sm.), **(f)** 6th position (150° dim. 30° sm.), **(g)** 7th position (180° dim. 0° sm.)

2.1 Uncertainty Analysis

The results of various wind tunnel tests for an identical configuration with the same set of flow parameters can be scattered due to numerous inevitable disturbances. A set of accurate data has been obtained by repeating the experiment. An analysis of the AF1300Z Balance was conducted to ensure satisfactory drag force data. Randomness has been identified, and errors mitigated by recording extensive data in the wind tunnel experiment. However, systematic errors may be introduced by the instrumentation used to measure the relevant axial force factors. To determine the accuracy of the AF1300Z balance, drag force values for a 24 mm diameter cylinder have been recorded as the air velocity increased from 0 m/s to 22.184 m/s. Afterward, the air

velocity was reduced from 22.184 m/s to 0 m/s and again drag was recorded during this decreasing velocity. Variation in the measured drag force has been observed during both phases of velocity change. Fig.7 displays the comparison of the drag forces on the cylinder during both increases and decreases in air velocity. Remarkably similar drag force values have been recorded in both cases, confirming the accuracy of the AF1300Z Balance readings. Thus, in subsequent experiments, readings were taken during the wind speed increase.

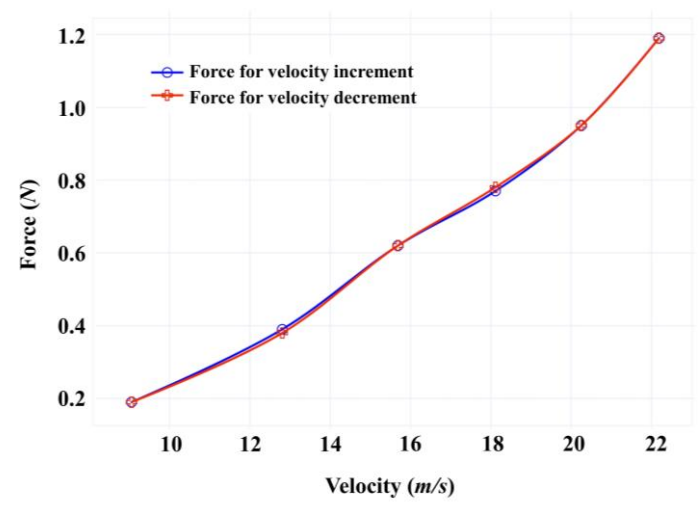


Fig.7 Drag forces on the cylinder at increasing wind speed and decreasing wind speed

3. Result and Discussion

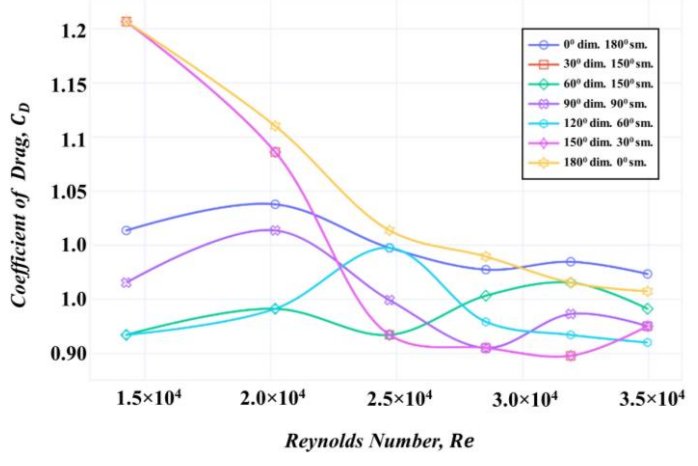


Fig.8: C_D vs. Re for seven different positions of the dimpled surface on the cylinder

The drag coefficient for various surface configurations of a cylinder with combinations of dimpled (dim.) and smooth (sm.) surfaces is presented in **Fig.8**, with data plotted across a range of Reynolds Numbers. This study aimed to understand the impact of different dimple placements on drag reduction. The following observations and interpretations can be derived from the results:

General Trend in Drag Coefficients:
 Across all configurations, a general reduction in the drag coefficient was observed as the Reynolds Number increases. This trend aligns with classical aerodynamic behavior, where increasing flow velocity promotes a

transition in the boundary layer from laminar to turbulent flow, delaying flow separation and reducing drag. The decreasing values suggested effective control over boundary layer behavior, especially as dimples disrupted the laminar layer, promoting localized turbulence and an earlier transition to turbulent flow.

Optimal Dimple Placement for Drag Reduction:

The configuration with 60° dimpled and 150° smooth surface coverage displayed the lowest drag coefficient across most of the Reynolds Number range, particularly between 2.5×10⁴ and 3.5×10⁴. This placement of dimples on the windward side appeared effective in delaying flow separation and reducing the pressure drag by managing the boundary layer transition effectively. This outcome supports the hypothesis that partial dimple coverage, strategically placed on the windward side, can optimize drag reduction by creating localized turbulence to suppress separation.

As dimple coverage increased on the windward side (e.g., 90° dim., 90° sm. and 120° dim., 60° sm. configurations), C_D values showed a consistent reduction at higher Reynolds Numbers. This observation suggested that increased dimple coverage enhanced turbulent mixing over the cylinder surface, effectively delaying flow separation at higher flow velocities. The 120° dim., 60° sm. configuration performed particularly well at high Re values, making it a favorable option for drag reduction in conditions involving higher flow speeds.

4) Highest Drag Coefficient in Limited Dimple Coverage Configurations:

The configuration with 30° dimpled and 150° smooth surface coverage demonstrated the highest drag coefficient, especially in the lower Reynolds Number range (~1.5×10⁴), reaching a C_D of approximately 1.2. This configuration provided limited dimple coverage, likely insufficient to influence boundary layer behavior significantly, leading to earlier flow separation and higher drag. These results suggested that minimal dimpled coverage on the windward side may not be effective for drag reduction due to inadequate disturbance to the boundary layer.

5) Comparison Between Full Dimpled and Full Smooth Configurations:

The 180° dimpled, 0° smooth configuration showed a high drag coefficient at lower Re values, similar to fully smooth configurations, but displayed a sharper decrease as the Reynolds Number increased. By Re= 3.0×10^4 , its C_D was comparable to other dimpled configurations, suggesting that a fully dimpled surface may reduce drag at higher flow velocities. However, the higher initial C_D values indicated that fully dimpled configurations might be less efficient at lower flow speeds compared to configurations with selective dimple coverage.

Among all configurations, 60° dim., 150° sm. and 120° dim., 60° sm. were the most effective in reducing drag, especially at higher Re. The results imply that targeted dimple placement, particularly with a substantial but not fully dimpled surface on the windward side, can enhance drag reduction by effectively managing flow separation and pressure drag.

6. Conclusion

The study demonstrated that optimized dimple placements on a cylinder surface can significantly influence drag characteristics. Configurations with selective windward side dimpling (such as 60° dim., 150° sm. and 120° dim., 60° sm.) consistently reduced drag at high Reynolds Numbers, highlighting their potential for applications in aerodynamic and hydrodynamic systems where flow-induced drag is a critical factor. Further studies can expand on these findings by exploring dimple depth and arrangement to refine drag reduction strategies further.

Acknowledgement

We would like to express our sincere gratitude to the Department of Mechanical and Production Engineering at Ahsanullah University of Science and Technology (AUST) for granting us access to the wind tunnel facility in the Fluid Mechanics Laboratory.

References

- [1] M.W. Jones, G.P. Peters, T. Gasser, R.M. Andrew, C. Schwingshackl, J. Gütschow, R.A. Houghton, P. Friedlingstein, J. Pongratz, C. Le Quéré, National contributions to climate change due to historical emissions of carbon dioxide, methane, and nitrous oxide since 1850, Sci Data 10 (2023) 155.
- [2] P. Bearman, Bluff Body Flow Research with Application to Road Vehicles, in: 2009: pp. 3–13.
- [3] Y.F. Fu, C.Q. Yuan, X.Q. Bai, Marine drag reduction of shark skin inspired riblet surfaces, Biosurf Biotribol 3 (2017) 11–24.
- [4] K. Chen, Z. Mo, J. Hang, The recirculation flow after different cross-section shaped high-rise buildings with applications to ventilation assessment and drag parameterization, Build Simul 17 (2024) 509–524.
- [5] P. Mallikarjuna, Ch.S. Babu, T. Murali, M.R. Satish Kumar, BRIDGE PIERS—DRAG FORCE COEFFICIENTS, ISH Journal of Hydraulic Engineering 10 (2004) 48–55.
- [6] H. Tian, Review of research on high-speed railway aerodynamics in China, Transportation Safety and Environment 1 (2019) 1–21.
- [7] S. Gudmundsson, Aircraft Drag Analysis, in: General Aviation Aircraft Design, Elsevier, 2022: pp. 657–752.
- [8] P.W. Bearman, J.K. Harvey, Control of circular cylinder flow by the use of dimples, AIAA Journal 31 (1993) 1753–1756.
- [9] F.G. Howard, W.L. Goodman, Axisymmetric bluff-body drag reduction through geometrical modification, J Aircr 22 (1985) 516–522.

- [10] C. Tay, Determining the Effect of Dimples on Drag in a Turbulent Channel Flow, in: 49th AIAA Aerospace Sciences Meeting Including the New Horizons Forum and Aerospace Exposition, American Institute of Aeronautics and Astronautics, Reston, Virigina, 2011.
- [11] Y. Eng, C.M.J. Tay, B.C. Khoo, On Drag Reduction and Heat Transferin Turbulent Channel Flow over Circular Dimples: The Shift of the Deepest Point of Dimples, in: Proceedings of the 6th World Congress on Momentum, Heat and Mass Transfer, Avestia Publishing, 2021.
- [12] H. Lienhart, M. Breuer, C. Köksoy, Drag reduction by dimples? A complementary experimental/numerical investigation, Int J Heat Fluid Flow 29 (2008) 783–791.
- [13] K. Klausmann, B. Ruck, Drag reduction of circular cylinders by porous coating on the leeward side, J Fluid Mech 813 (2017) 382–411.
- [14] M. van Nesselrooij, L.L.M. Veldhuis, B.W. van Oudheusden, F.F.J. Schrijer, Drag reduction by means of dimpled surfaces in turbulent boundary layers, Exp Fluids 57 (2016) 142.
- [15] J. Choi, W.-P. Jeon, H. Choi, Mechanism of drag reduction by dimples on a sphere, Physics of Fluids 18 (2006).
- [16] B. Zhou, X. Wang, W. Guo, W.M. Gho, S.K. Tan, Control of flow past a dimpled circular cylinder, Exp Therm Fluid Sci 69 (2015) 19–26.
- [17] F. Yan, H. Yang, L. Wang, Study of the Drag Reduction Characteristics of Circular Cylinder with Dimpled Surface, Water (Basel) 13 (2021) 197.

NOMENCLATURE

 F_D : Drag force, N

 C_D : Drag Coefficient, []

 V_{∞} : Velocity of air, m/s²

Re: Reynolds Number, []

 ρ_{mf} : Density of manometric fluid, kg/m³

 ρ_{air} : Density of air, kg/m³

D: Diameter of the Cylinder, m

d: Depth of the dimple, m

D/d: Depth-to-diameter ratio, []

L: Length of the cylinder, m

 H_{air} : Manometric Column Height of air, m A: Cross-sectional Area of the Cylinder, m²